Photoneutron cross section measurements on ^{65}Cu: toward understanding (n, γ) cross sections relevant to weak s-process nucleosynthesis*

Yu-Long Shen (谌雨龙)[1,2,3] Zi-Rui Hao (郝子锐)[2#] Qian-kun Sun (孙乾坤)[4,5] Hong-Wei Wang (王宏伟)[2,5]
Long-Xiang Liu (刘龙祥)[2] Hang-Hua Xu (许杭华)[2,5] Yue Zhang (张岳)[2] Sheng Jin (金晟)[4,5]
Kai-Jie Chen (陈开杰)[4,6] Meng-Die Zhou (周梦蝶)[2,7] Zhen-Wei Wang (王振伟)[4,5] Meng-Ke Xu (徐孟轲)[4,5]
Xiang-Fei Wang (王向飞)[4,5] Chang Yang (杨畅)[2,8] Pu Jiao (焦普)[7] Chun-Wang Ma (马春旺)[9]
Gong-Tao Fan (范功涛)[2,5†] Zhi-Cai Li (李志才)[1,3‡] Wen Luo (罗文)[1,3§]

[1]School of Nuclear Science and Technology, University of South China, Hengyang 421001, China
[2]Shanghai Advanced Research Institute, Chinese Academy of Sciences, Shanghai 201210, China
[3]Key Laboratory of Advanced Nuclear Energy Design and Safety, Ministry of Education, Hengyang 421001, China
[4]Shanghai Institute of Applied Physics, Chinese Academy of Sciences, Shanghai 201800, China
[5]University of Chinese Academy of Sciences, Beijing, 101408, China
[6]School of Physical Science and Technology, ShanghaiTech University, Shanghai 201210, China
[7]College of Physics, Henan Normal University, Xinxiang 453007, China
[8]China Nuclear Data Center, China Institute of Atomic Energy, Beijing 102413, China
[9]Institute of Nuclear Science and Technology, Henan Academy of Sciences, Zhengzhou 450046, China

Abstract: A new measurement of the ^{65}Cu(γ, n)^{64}Cu photoneutron cross section is performed using quasi-monoenergetic, tunable γ-ray beams produced at the Shanghai Laser Electron Gamma Source (SLEGS). The energy spectrum of the SLEGS γ-ray beams incident on the isotopically enriched ^{65}Cu target is monitored using a BGO detector, while the photoneutron yields are determined with a moderated ^{3}He detection array with high and flat efficiency. Within the energy range of $10.1 \leq E_\gamma \leq 17.6$ MeV, the measured $\sigma(E_\gamma)$ data have an uncertainty of $\lesssim 4\%$, and a pronounced giant-dipole peak is observed at $E_\gamma \simeq 16.65$ MeV with a maximal cross section of $\sigma_{\rm max} \simeq 137$ mb. These photoneutron data are compared with previous experimental results and are employed to extract the γ-ray strength function of ^{65}Cu above the neutron threshold. Furthermore, we calculate the radiative neutron capture cross sections and astrophysical reaction rates for ^{64}Cu, which is a short-lived intermediate nucleus whose reaction rate controls the local abundance distribution in the weak s-process. It is found that the calculated ^{64}Cu(n, γ)^{65}Cu data have an overall agreement with ENDF/B-VIII.0, JEFF-3.3, and TENDL-2023 evaluations, and the corresponding astrophysical reaction rates are consistent with those reported in the JINA REACLIB database.

Keywords: partial photoneutron cross sections, ^{65}Cu, TALYS, laser Compton scattering γ-ray, Bayesian optimization.

DOI: 10.1088/1674-1137/ae5a18 **CSTR:** 32044.14.ChinesePhysicsC.50064002

I. INTRODUCTION

Photonuclear data, which describe the response of atomic nuclei to incident photons, are essential for fundamental nuclear physics and have broad applications across various fields [1]. The (γ, n) cross sections are a branch of photonuclear data and can be used to calculate the γ-ray strength function (γSF) [2, 3], with which γ-ray cascades in nuclear reactions can be described [4, 5]. At photon energies between 10 and 20 MeV, nuclear reactions are generally dominated by the Giant Dipole Resonance (GDR), which is interpreted as a collective oscilla-

Received 10 February 2026; Accepted 26 March 2026; Accepted manuscript online 27 March 2026

* This work was supported by the National Key Research and Development Program (2023YFA1606901), and the National Natural Science Foundation of China (12575133, 12505144)

† E-mail: fangt@sari.ac.cn
‡ E-mail: lizhicai@usc.edu.cn
§ E-mail: wenluo-ok@163.com
# These authors contributed equally as the first authors

tion of protons against neutrons [6]. The (γ, n) cross sections measured in the GDR region provide access to key nuclear properties [7, 8] and are crucial for improving models of nuclear structure and reaction mechanisms, such as Hauser-Feshbach (HF) statistical calculations [9, 10].

It is known that weak slow process (*s*-process) associated with helium burning in massive stars (with masses exceeding approximately eight solar masses) dominates the synthesis of nuclei in the mass range $60 < A < 90$. The overall abundance distribution in this region is particularly sensitive to the cross sections of the Ni-Cu-Zn isotopes, which lie at the onset of the *s*-process path. The photoneutron cross section of the stable isotope ^{65}Cu and neutron-capture cross section of the unstable isotope ^{64}Cu (with a half-life of 12.7 h) may affect the abundances of ^{64}Ni and ^{66}Zn, which are neighboring stable nuclides around ^{65}Cu in the mass region involved in the weak *s*-process [11]. Fig. 1 illustrates the primary reaction pathways involving ^{64}Cu and ^{65}Cu. Therefore, precise experimental constraints on these key reactions become essential for improving the reliability of nucleosynthesis models in the weak *s*-process mass region. In addition, the ^{65}Cu(γ, n)^{64}Cu reaction represents a candidate route for the production of medically interesting isotope ^{64}Cu.

Experimental and theoretical investigations of photonuclear reactions on ^{65}Cu have been extensively reported [12−16], providing a few sets of photonuclear reaction data. However, visible discrepancies still exist among available measurements due to the usage of both different γ-ray sources (such as bremsstrahlung radiations and quasi-monoenergetic γ-ray beams) and experimental techniques (such as direct measurements [17] and subtraction methods [15]). These inconsistencies are reflected in both the profile of the energy differential cross section (distribution width and peak position*n*) and the value of its peaked cross section. Therefore, a new direct measurement employing quasi-monoenergetic γ-ray beams together with an isotopically enriched target is urgently needed to improve the reliability of ^{65}Cu(γ, n)^{64}Cu data, which may in turn enable a reliable calculation of the inverse ^{64}Cu(n, γ)^{65}Cu cross sections.

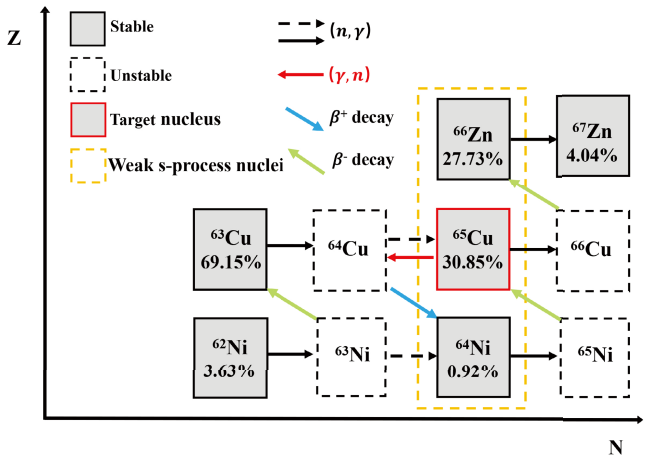

Fig. 1. (color online) Partial reaction path in the vicinity of ^{65}Cu. Stable isotopes are shown in gray, while unstable ones are in white. Red and black arrows represent photoneutron reactions and inverse neutron capture reactions, respectively, while green and blue arrows indicate β^- and β^+ decays, respectively.

In this paper, we report a detailed experimental investigation on the photoneutron reaction of isotopic ^{65}Cu using quasi-monoenergetic and energy-tunable γ-ray beams. The measured ^{65}Cu(γ, n)^{64}Cu data are presented, and the experimental and evaluated data are compared. In Sec. II, the experimental procedure is described. The analysis and discussion of the extracted photoneutron cross sections are presented in Sec. III. The radiative neutron capture cross sections and corresponding astrophysical reaction rates for the unstable isotope ^{64}Cu are calculated and compared with evaluated data in Sec. IV. Finally, conclusions are drawn in Sec. V.

II. EXPERIMENTAL PROCEDURE

Shanghai Laser Electron Gamma Source (SLEGS, https://cstr.cn/31124.02.SSRF.BL03SSID) is a beamline designed to produce energy-tunable MeV γ-ray beams through backward or slanting laser-Compton scattering (LCS) between CO_2 laser photons (with wavelength λ = 10.64 μm) and 3.5 GeV electrons from Shanghai Synchrotron Radiation Facility (SSRF) [18, 19]. The SLEGS γ-ray energy can be adjusted from 21.7 to 0.66 MeV by varying the laser incident angle at 180° and within the range of 20°−160°. After the successful commissioning in 2021 [20], the final configuration of the SLEGS beamline was opened to users in 2023 with the installation of the Three-hole (T) collimator [21, 22], which controls the energy resolution and flux of γ-ray beams. The energy profile and flux were systematically investigated to characterize γ-ray beams produced at SLEGS [23−28]. Now, the SLEGS γ-ray beams have a medium energy resolution, primarily due to the large angular dispersion of laser beams with a short focal length inside the interaction chamber [26, 29]. The energy resolution is achieved by using the T collimator with a 2 mm aperture. Fig. 2(a) shows the SLEGS beamline configuration and the following detector setup at the end of the beamline. Fig. 2(b) shows the schematic interaction geometry of the SSRF electron beam and CO_2 laser pulse in the laboratory frame. Fig. 2(c) shows the SLEGS γ-ray profile diagnosed after they pass through the T collimator. In the experiment, the copper attenuator was positioned sufficiently far from the detector system, with its front end located 290 cm from the FED detector and its rear end 130 cm from the BGO detector, such that no obvious

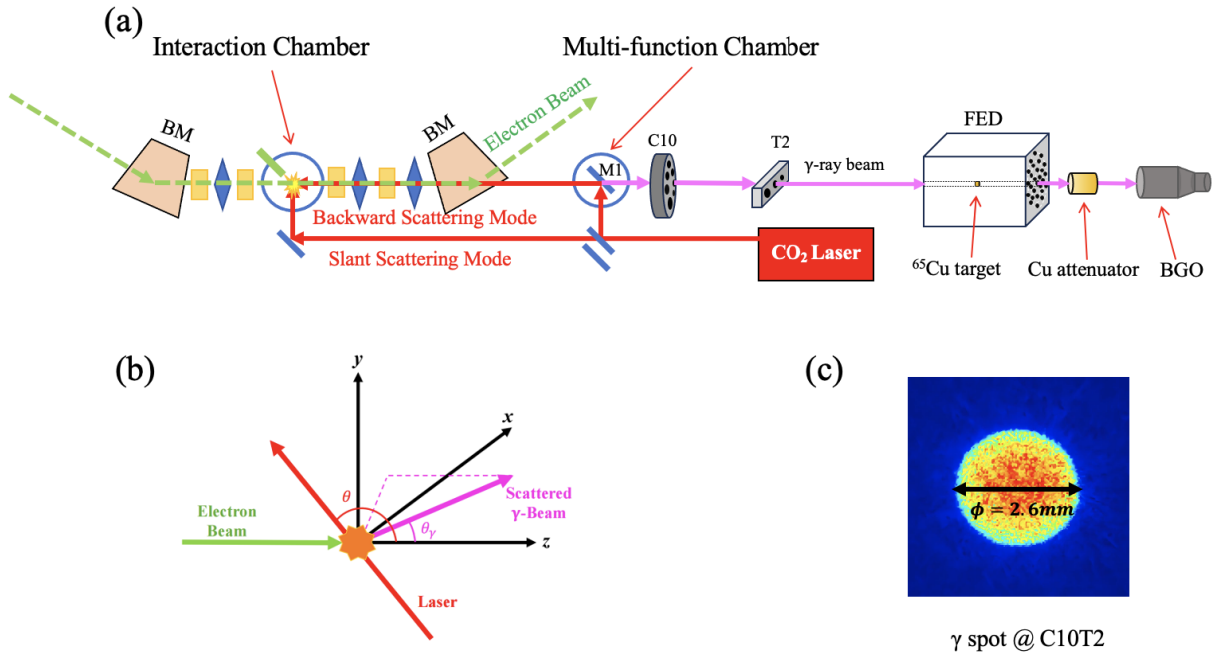

Fig. 2. (color online) (a) Schematic diagram of the ^{65}Cu(γ, n) cross section measurement setup. (b) Interaction geometry of an electron beam and laser beam in the laboratory frame, from which the LCS γ-rays are emitted within a small cone angle along the electron moving direction. (c) LCS γ-ray profile diagnosed after passing through a 10 mm-aperture coarse collimator and 2 mm-aperture T collimator.

background contribution from the attenuator to the FED was observed.

In this study, the SLEGS γ-ray beams were produced under the operation of slanting LCS mode. These γ-ray beams exactly cover the energy range from the single-neutron separation energy ($S_n = 9.91$ MeV) up to the double-neutron separation threshold ($S_{2n} = 17.82$ MeV). After collimation, the SLEGS γ-ray beams were irradiated on the ^{65}Cu target, which was precisely positioned at the geometric center of the flat-efficiency detector (FED). The photon-induced neutrons were then moderated by polyethylene before being captured by the ^{3}He proportional counters. The penetrated γ-ray beams were attenuated by a copper attenuator and subsequently measured with a BGO detector. Digital signal processing was performed using the Mesytec MDPP-16 [30] in conjunction with an MVME-based data acquisition (DAQ) system [31].

A. γ-ray spectrum

During ^{65}Cu irradiation, the γ-ray spectrum after attenuation was continuously monitored using a BGO detector positioned downstream of the target. A representative spectrum measured at a laser incident angle of $\theta_L = 90°$ is shown in Fig. 3(a). After obtaining the BGO measured spectrum (black solid line), the SLEGS γ-ray spectrum (red dashed line) incident on the target was calculated by considering the thickness and attenuation coefficients of both the copper attenuator and target material. The spectral distribution was unfolded using a direct unfolding method based on the detector response matrix simulated with GEANT4 [32]. The blue dashed line in Fig. 3(a) represents the reconstructed spectrum, which is obtained by folding the incident gamma spectrum with the detector response matrix, showing good agreement with the measured BGO response spectrum. The total number of γ-rays contributing to the reaction, N_γ, was obtained by integrating the incident gamma spectrum above S_n, as shown by the red shaded region of Fig. 3(a). The unfolded energy profiles for the γ-ray beams used in the ^{65}Cu measurements are shown in Fig. 3(b). The intensity difference between the measured and unfolded spectra is mainly caused by a significant attenuation from both the copper attenuator (160 mm thickness) and ^{65}Cu target during experiment (5 h).

B. ^{65}Cu target

The physical parameters of the ^{65}Cu target are listed in Table 1.The target purity was determined by an inductively coupled plasma-mass spectrometer. The thickness uncertainty was estimated to be 0.01 %.

C. Neutron detection

Neutron counts (N_n) were determined with the FED. It consists of 26 ^{3}He proportional counters embedded in a polyethylene moderator with dimensions of 450 mm × 450 mm× 550 mm. This polyethylene moderator is covered with a 2 mm thick Cd sheet to absorb environ-

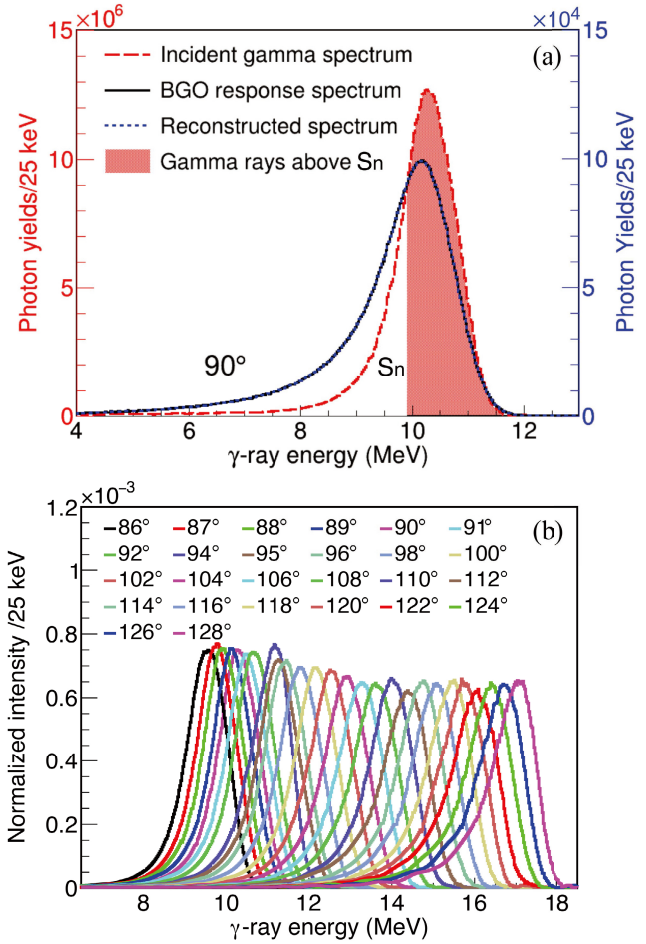

Fig. 3. (color online) (a) Typical γ-ray spectra measured by the BGO detector (see black line), folded-back γ-ray spectra (see blue line), and corresponding γ-ray spectra incident on the target (see red line) at θ_L = 90°. (b) Spectral distributions of the γ-ray beams unfolded at different θ_L.

mental neutrons and then further wrapped with a 50 mm thick layer of polyethylene. The proportional counters were arranged in three concentric rings to determine the average neutron energy via the ring-ratio (RR) method [33]. The inner ring, positioned at 65 mm from the center, contains 6 1-inch counters. The middle ring (110 mm from center) has 8 2-inch counters, and the outer ring (175 mm from center) holds 12 2-inch counters. All the proportional counters were filled with 2 atm of ^{3}He gas. The total FED efficiency in the plateau region was approximately 40%. The FED was calibrated using a ^{252}Cf neutron source, and its efficiency uncertainty was determined to be 3.02% [34].

The DAQ system of the FED enables recording of the pulse height and timestamp of signals from detectors. For N_n determination, accurate thresholds of the analog-to-digital converter spectra for each ^{3}He proportional counter were assigned to distinguish the γ background from the neutrons. Then, the constant bremsstrahlung-induced

Table 1. Parameters of the ^{65}Cu target used for irradiation.

Chemical purity Cu ~ 100.00 (%)			
Isotopic enrichment of ^{65}Cu ≥ 99.70 (%)			
Weight/mg	Diameter/mm	Thickness/mm	Density/ (g·cm^{-3})
529.34	10.000	0.88	7.59

background was distinguished from the LCS γ beam-induced neutrons by its time distribution [34]. In this work, the CO_2 laser operated at an average power of 5 W, with a pulse period of 1000 μs and pulse width of 50 μs. N_n can be extracted by directly subtracting the time normalized background. This method, as presented in our previous work [35], provides a practical approach to estimating the average neutron energy, which can then be used to determine the FED efficiency for detecting the neutrons emitted from ^{65}Cu(γ, n)^{64}Cu reactions.

III. DATA ANALYSIS AND RESULTS

A. Uncertainty of measured (γ, n) cross section

The total experimental uncertainties included statistical, methodological, and systematic uncertainties. The statistical uncertainty was primarily induced by N_n and N_γ, which encompass the corresponding statistical fluctuations. Because the incident N_γ had a sufficiently high count rate in our study, it contributed negligibly to the statistical uncertainty. The methodological uncertainty consists of two main components: the N_n extraction algorithm and unfolding procedure using the simulated BGO response matrix. The systematic uncertainties were primarily due to the external γ-ray induced by the copper attenuator, target thickness, and FED detection efficiency. The methodological uncertainty and systematic uncertainties are summarized in Table 2.

B. Folded cross section

The experimental photoneutron cross section $\sigma_{\rm exp}$ measured with quasi-monochromatic γ-ray beams is given by the following expression [36, 37]:

$$\sigma_{\rm exp} = \int_{S_n}^{E_{\rm max}} n_\gamma(E_\gamma)\sigma(E_\gamma){\rm d}E_\gamma = \frac{N_n}{N_\gamma N_t \xi \epsilon_n g}, \quad (1)$$

where $n_\gamma(E_\gamma)$ represents the normalized energy profile of the incident γ-ray beams. The term $\sigma(E_\gamma)$ denotes the monochromatic cross section, which is the quantity to be determined. N_n corresponds to the number of detected neutrons, while N_γ is the number of γ-rays incident on the ^{65}Cu target above S_n. The average FED efficiency, ϵ_n, is derived using the RR technique [35]. N_t represents the number of target nuclei per unit area. The correction factor in the target self-attenuation term is given by

Table 2. Methodological and systematic uncertainties.

	Parameter	Value (%)
Methodological	N_n extraction algorithm	2.0
	Unfolding method	1.0
Systematic	Target thickness	<0.1
	Copper attenuator	0.5
	FED efficiency	3.02

$\xi = (1-\mathrm{e}^{-\mu t})/(\mu t)$, where μ is the attenuation coefficient for incident γ-ray, and t is the target thickness. Finally, g is the fraction of the γ-ray flux above S_n (see Fig. 3(a)). Its expression is given by

$$g = \frac{\int_{S_n}^{E_{\max}} n_\gamma(E_\gamma)\mathrm{d}E_\gamma}{\int_0^{E_{\max}} n_\gamma(E_\gamma)\mathrm{d}E_\gamma}. \tag{2}$$

Note that the measured quantities described above are commonly referred to as monochromatic approximations. In reality, they correspond to the convolution of the true energy-dependent cross sections with the spectral distribution of the incident photon beam. Specifically, the measured cross section represents the folding of the excitation function with the γ-ray energy spectrum, which is the monochromatic approximation cross section in the experiment.

C. Monochromatic cross section

To obtain the energy-dependent photoneutron cross section $\sigma(E_\gamma)$, it is essential to extract it from the integral form given in Eq. (1). Each measured cross section represents a convolution of the true cross section $\sigma(E_\gamma)$ with the normalized incident beam profile $n_\gamma(E_\gamma)$. In this study, we adopted the unfolding algorithm proposed in Ref. [38] to extract $\sigma(E_\gamma)$ from Eq. (1):

$$\sigma_\mathrm{f} = \boldsymbol{D}\sigma, \tag{3}$$

where the quantity σ_f represents a monochromatic approximated cross section array with each element corresponding to the monochromatic approximated cross section measured at discrete beam energies (E_γ). The array σ contains the monochromatic cross sections. The matrix $\boldsymbol{D}$ is constructed from the normalized spectral distribution of the incident γ-ray beams with energy spanning from S_n to $E_{\max}$ at each independent measurement. Eq. (4) is the expanded form of Eq. (3). The number of rows (N) in $\boldsymbol{D}$ corresponds to the number of discrete beam energies, while the number of columns (M) represents the number of bins within the incident γ-ray spectrum. For the ^{65}Cu case, we choose $N = 25$ and $M = 1000$.

$$\begin{bmatrix}\sigma_1\\ \sigma_2\\ \vdots\\ \sigma_N\end{bmatrix}_\mathrm{f} = \begin{bmatrix} D_{11} & D_{12} & \cdots & \cdots & D_{1M}\\ D_{21} & D_{22} & \cdots & \cdots & D_{2M}\\ \vdots & \vdots & \vdots & \vdots & \vdots\\ D_{N1} & D_{N2} & \cdots & \cdots & D_{NM}\end{bmatrix}\begin{bmatrix}\sigma_1\\ \sigma_2\\ \vdots\\ \vdots\\ \sigma_M\end{bmatrix}. \tag{4}$$

An unfolding iteration method is employed to extract the monochromatic cross section σ:

(1) As our starting point, we choose a constant trial function σ^0 for the zeroth iteration. This initial vector is multiplied with $\boldsymbol{D}$, and we get the zeroth folded vector $\sigma_\mathrm{f}^0 = \boldsymbol{D}\sigma^0$.

(2) The next trial input function, σ^1, is established by adding the difference of the experimentally measured spectrum, σ_exp, and the folded spectrum, σ_f^0, to σ^0:

$$\sigma^1 = \sigma^0 + (\sigma_\mathrm{exp} - \sigma_\mathrm{f}^0). \tag{5}$$

It is worth noting that the dimension of σ^0 (M) is much larger than those of σ_exp and σ_f^0 (N). To solve Eq. (5), it is necessary to expand the dimensions of σ_exp and σ_f^0 to M by interpolation.

(3) The above steps are iterated i times, giving

$$\sigma_\mathrm{f}^i = \boldsymbol{D}\sigma^i, \tag{6}$$

and

$$\sigma^{i+1} = \sigma^i + (\sigma_\mathrm{exp} - \sigma_\mathrm{f}^i). \tag{7}$$

The χ^2 value between σ_exp and σ_f^{i+1} is recorded in each iteration. The iterative process is stopped once convergence is achieved. This means that $\sigma_\mathrm{f}^{i+1} \approx \sigma_\mathrm{exp}$ within statistical uncertainties.

Figure 4 presents the monochromatic cross sections σ_exp and unfolded energy-dependent cross sections $\sigma(E_\gamma)$ for the ^{65}Cu(γ, n)^{64}Cu reaction. The $\sigma(E_\gamma)$ values at each E_γ, together with their uncertainties, are summarized in Table 3. These uncertainties account for statistical, systematic, and methodological contributions. In our case, the total uncertainty of the unfolded $\sigma(E_\gamma)$ is approximately 4%, except in the low-energy region of $S_n < E_\gamma < 10.90$ MeV, where $\sigma(E_\gamma)$ drops below 12.10 mb.

D. ^{65}Cu(γ, n)^{64}Cu reaction cross section

We compare the currently measured data for the ^{65}Cu(γ, n)^{64}Cu reaction with available experimental data from the EXFOR database [12−15] and TENDL-2023 evaluations. The results are shown in Fig. 5(a). Because

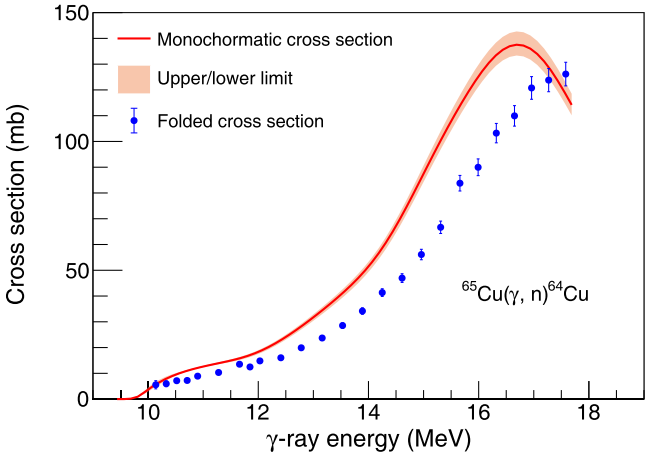

Fig. 4. (color online) ^{65}Cu(γ, n)^{64}Cu cross section as a function of the incident γ-ray energy, E_γ. The dots represent the folded cross section, and the line with a shaded area shows the monochromatic cross section.

Table 3. Monochromatic cross sections and corresponding uncertainties for the ^{65}Cu(γ, n)^{64}Cu reaction.

E_γ/MeV	σ/mb	Statistical uncertainty /mb	Methodological uncertainty /mb	Systematic uncertainty /mb	Total uncertainty /mb
10.14	5.69	1.61	0.10	0.18	1.62
10.33	7.92	1.45	0.15	0.25	1.48
10.52	9.62	0.42	0.17	0.30	0.55
10.71	10.99	0.36	0.20	0.35	0.54
10.90	12.10	0.63	0.22	0.38	0.77
11.28	13.92	0.22	0.24	0.44	0.55
11.66	15.80	0.25	0.27	0.50	0.62
11.85	17.06	0.19	0.28	0.54	0.63
12.03	18.65	0.30	0.30	0.59	0.72
12.41	22.92	0.22	0.37	0.72	0.84
12.78	28.30	0.26	0.45	0.89	1.03
13.16	34.39	0.29	0.55	1.08	1.25
13.53	41.06	0.32	0.65	1.29	1.48
13.89	48.81	0.34	0.79	1.54	1.76
14.25	58.75	0.39	0.94	1.85	2.11
14.61	71.48	0.45	1.14	2.25	2.57
14.96	85.98	0.59	1.40	2.71	3.11
15.31	100.46	0.59	1.64	3.17	3.62
15.66	113.67	0.65	1.88	3.58	4.10
15.99	125.08	0.75	2.06	3.94	4.51
16.32	133.59	1.00	2.22	4.21	4.87
16.65	137.36	0.91	2.25	4.33	4.97
16.96	135.58	0.81	2.34	4.27	4.94
17.27	128.65	0.77	2.20	4.06	4.68
17.58	118.45	0.72	2.00	3.73	4.30

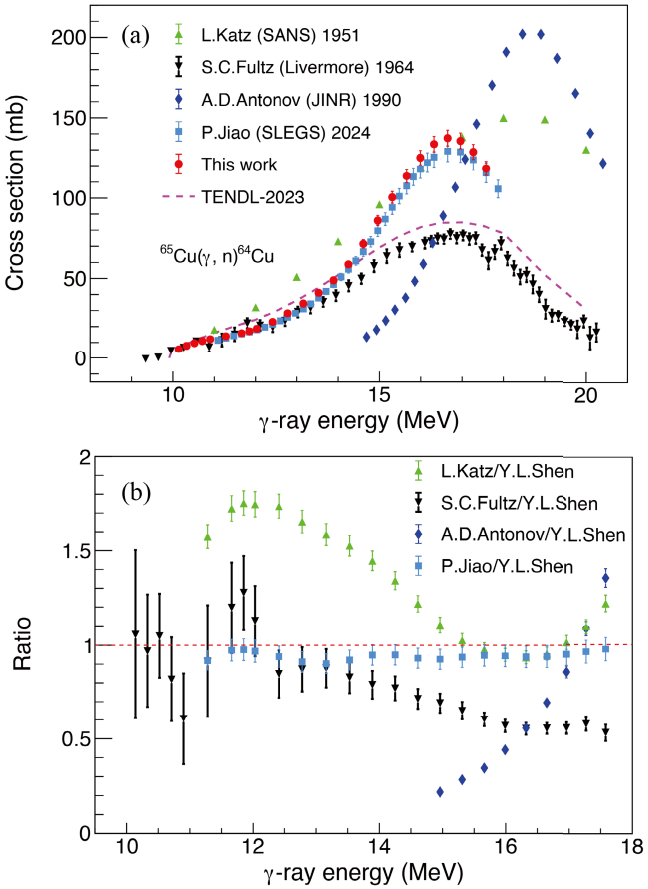

Fig. 5. (color online) (a) Unfolded cross section curve for the ^{65}Cu(γ, n)^{64}Cu reaction together with available experimental and evaluated (γ, n) data [12−15]. (b) Ratios of the present cross sections to those of experimental data.

earlier measurements employed different types of γ-ray sources together with different experimental techniques, their results are analyzed and discussed separately. To quantitatively analyze these differences, we further calculate the ratios of the data obtained in the current study to the experimental data shown in Fig. 5(b).

Katz *et al.* [12] reported ^{65}Cu photoneutron cross sections at the SANS laboratory in Canada in 1951, using bremsstrahlung photons with endpoint energies between 11.00 and 22.00 MeV. Antonov *et al.* [13] performed a similar measurement at JINR in Russia with bremsstrahlung radiation endpoint energies ranging from 14.68 to 24.55 MeV. Compared with the results in the present work, both datasets show substantial deviations at lower energies and within the GDR peak region. For example, a significant difference exists in their GDR peak positions, magnitudes, and widths.

Fultz *et al.* [14] measured the ^{65}Cu(γ, n)^{64}Cu data at the Livermore Laboratory in 1964 using quasi-monoenergetic annihilation photons and a BF_3-filled FED neutron detector, covering the energy range of 9.34−27.78 MeV. This measurement exhibits a good agreement with our

data below 15 MeV, although the data of Fultz *et al*. remain systematically lower than our data by a factor of approximately 0.4 in the GDR region.

Recently, Jiao *et al*. [15] performed the photoneutron cross section measurement with a natural Cu target using the quasi-monoenergetic γ-ray beams at the SLEGS. Combining the measured natural Cu data and previously measured ^{63}Cu data [39], the ^{65}Cu(γ, n)^{64}Cu cross sections within the energy range of 11.28−17.58 MeV were successfully extracted using the subtraction method [15]. Their result shows good agreement with the present measurement using an isotopic ^{65}Cu target, as shown in Fig. 5.

We should note that early measurements with bremsstrahlung γ-ray sources [12, 13] suffered from limited accuracy due to the broad photon spectra and additional uncertainties introduced in the unfolding procedures. Although the Livermore data were obtained using quasi-monoenergetic annihilation photons, systematic discrepancies still appear when compared with the Saclay measurements that employed the same type of γ-ray beams. The SLEGS experiment [15] did not measure the cross sections near S_n of ^{65}Cu, which led to a slight difference between the monochromatic cross sections obtained through the subtraction method and those from the present experiment.

IV. DISCUSSIONS

A. γ-ray strength function of ^{65}Cu

γSF [40] is a nuclear statistical quantity used to describe the nuclear electromagnetic response. In the de-excitation mode, γSF quantifies the average probability of a nucleus emitting a γ-ray of a given energy E_γ during de-excitation, which we refer to as downward γSF and can be defined by [41]

$$\overleftarrow{f_{X1}}(E_\gamma) = \frac{\langle \Gamma_{X1}(E_\gamma)/E_\gamma^3 \rangle}{D_\ell}. \tag{8}$$

Here, the symbol X is either electric (E) or magnetic (M), $\langle \Gamma_{X1}(E_\gamma) \rangle$ is the average radiation width, and D_ℓ is the average level spacing for s-wave ($\ell = 0$) or p-wave ($\ell = 1$) neutron resonances.

In contrast, γSF in the excitation mode, which we refer to as upward γSF, is defined by the average cross section for $E1/M1$ photoabsorption $\langle \sigma_{X1}(E_\gamma) \rangle$ to the final states with all possible spins and parities [42]:

$$\overrightarrow{f_{X1}}(E_\gamma) = \frac{1}{3\pi^2\hbar^2c^2}\frac{\langle \sigma_{X1}(E_\gamma) \rangle}{E_\gamma}. \tag{9}$$

Here, $\hbar$ is the planck constant, and c is the speed of light in vacuum. Above S_n, except at energies very close to the reaction threshold, the total upward γSF can be approximated by replacing $\sigma_{X1}(E_\gamma)$ with experimental (γ, n) cross sections, which dominate the photoabsorption cross section in this energy region. This approach relies on the principle of the detailed balance [43] and on the generalized Brink hypothesis, which assumes that the average electromagnetic decay process (*i.e*., photo-deexcitation) can be directly related to the inverse photo-excitation and depends only on the energy of the emitted γ-ray, irrespective of the absolute excitation energy or nuclear structure properties such as spin and parity. This assumption is expressed as $f_{X1}(E_\gamma) = \overleftarrow{f_{X1}}(E_\gamma) = \overrightarrow{f_{X1}}(E_\gamma)$ and provides the theoretical foundation for linking the (γ, n) cross section to the downward γSF:

$$f_{E1}(E_\gamma) = \frac{1}{3\pi^2\hbar^2c^2}\frac{\sigma_{\gamma n}(E_\gamma)}{E_\gamma}, \tag{10}$$

where the constant $1/(3\pi^2\hbar^2c^2) = 8.674\times10^{-8}\,\mathrm{mb^{-1}\,MeV^{-2}}$. Using this relation, we can obtain the experimentally constrained γSF from the measured ^{65}Cu(γ, n)^{64}Cu data, as shown in Fig. 6. Note that Eq. (10) holds only when the neutron channel in the photoneutron data dominates. In the vicinity of S_n, the competing γ emission must be taken into account through the HF formalism.

We further performed a theoretical analysis for ^{65}Cu γSF using the TALYS software (version 2.0) [44]. Here, the $E1$ strength was described by the macroscopic Brink–Axel Lorentzian (BAL) model [45, 46], and the $M1$ strength was described using the default spin-flip and scissors mode [47] in TALYS. These results are also

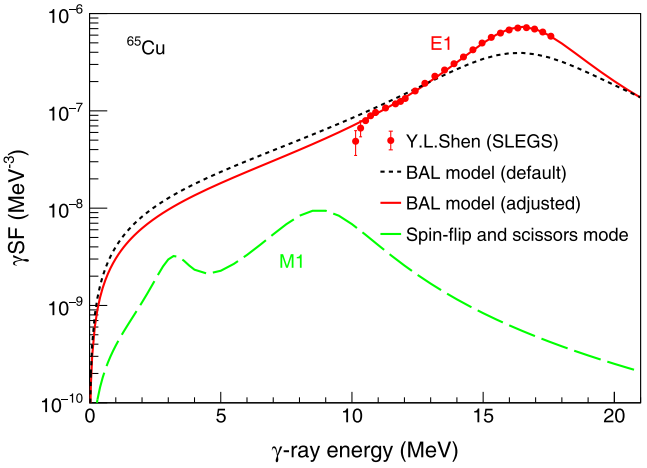

Fig. 6. (color online) Comparison of the experimentally extracted γSF (red circles) for ^{65}Cu with theoretical calculations. The black line corresponds to the $E1$ component calculated using the BAL model (strength 2), and the green line represents the $M1$ contribution arising from the spin-flip and scissors mode (strengthM1 3) in TALYS. The red line indicates the adjusted BAL model that fits the experimental data well.

shown in Fig. 6. It is found that the theoretical γSF, by default, and experimental data have noticeable discrepancies. This suggests that additional constraints are required to further improve the theoretical description.

To improve the agreement between the theoretical calculation and experimental data, the Lorentzian parameters *sgr*, *ggr*, and *egr* in TALYS calculations were adjusted simultaneously by a Bayesian optimization procedure [48, 49]. The parameter spaces were chosen in a proper way such that the calculated cross sections encompass the experimental upper and lower limits. Within this parameter space, we try to identify an optimal parameter set that best reproduces the experimentally extracted γSF, which corresponds to a minimized value for chi-square (χ^2) between the TALYS calculations and experimental data. In our case, χ^2 reads

$$\chi^2 = \frac{1}{N}\sum \frac{(\gamma\mathrm{SF}_{\mathrm{th}} - \gamma\mathrm{SF}_{\mathrm{exp}})^2}{\gamma\mathrm{SF}_{\mathrm{err}}^2}, \tag{11}$$

where N is the number of experimental data points, and $\gamma\mathrm{SF}_{\mathrm{th}}$, $\gamma\mathrm{SF}_{\mathrm{exp}}$, and $\gamma\mathrm{SF}_{\mathrm{err}}$ represent the theoretical data, experimental data, and uncertainty of experimental data, respectively. In our case, a Gaussian process was employed as a surrogate model to describe the dependence of χ^2 on model parameters in TALYS, assuming that these χ^2 values follow a Gaussian distribution. At each iteration, the next candidate point was selected by maximizing the expected improvement acquisition function. Then, an optimal parameter set was determined as the one that yields a globally minimum χ^2 among all data points. As the BAL model is employed, the χ^2 value for ^{65}Cu reaches a minimum of 9.96 when the Lorentzian parameters *sgr* = 139.31, *egr* = 16.63, and *ggr* = 4.37. One can see that the optimized calculation reproduces the experimental data of ^{64}Cu γSF well (see Fig. 6).

B. Radiative (n, γ) cross section for ^{64}Cu

The constrained ^{65}Cu γSF is further applied to calculate neutron capture cross sections for the inverse reaction ^{64}Cu(n, γ)^{65}Cu. Note that, in addition to the constrained γSF, the above calculation is highly sensitive to the nuclear level density (NLD) in TALYS. As a result, we first check the level density data considering different NLD models. Fig. 7 shows six kinds of level densities for ^{65}Cu, which are predicted by available NLD models: CTM [50], BFM [51], GSM [52, 53], HF-BCS [54], Skyrme-HFB [55], and Gogny-HFB [56]. One can see that these level density curves show an overall agreement, whereas a slight variation appears when the excitation energy is above 7 MeV.

By using the adjusted BAL model ($E1$) and the default spin-flip and scissors mode ($M1$), we further calculate radiative neutron capture cross sections for ^{64}Cu. The resulting ^{64}Cu(n, γ)^{65}Cu data are shown in Fig. 8. The

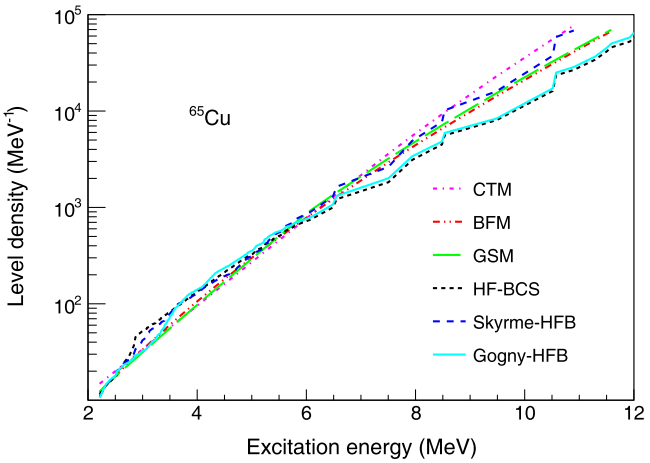

Fig. 7. (color online) Six NLD curves for ^{65}Cu calculated with CTM [50], BFM [51], GSM [52, 53], HF-BCS [54], Skyrme-HFB [55], and Gogny-HFB [56].

shaded band in the figure reflects the data uncertainty arising from different NLD models [38, 57]. Evaluated data from the EAF-2010, ENDF/B-VIII.0, JEFF-3.3, TENDL-2023, and JENDL-5 libraries are also presented in Fig. 8 for comparison. One can see that the data obtained within the BAL model show good agreement with the EAF-2010, TENDL-2023, and JENDL-5 evaluations, whereas they are higher than the evaluated data from both ENDF/B-VIII.0 and JEFF-3.3.

C. Astrophysical reaction rate

According to the ^{64}Cu(n, γ)^{65}Cu data presented above, the corresponding astrophysical reaction rates were calculated. Fig. 9(a) shows the ^{64}Cu(n, γ)^{65}Cu reaction rate as a function of astrophysical temperature, together with the

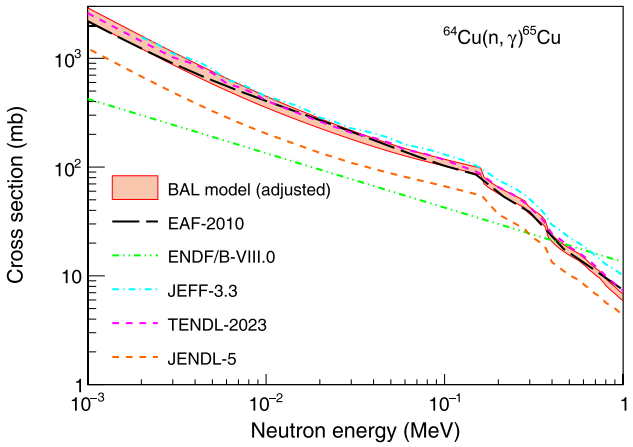

Fig. 8. (color online) Comparison of the ^{64}Cu(n, γ)^{65}Cu cross sections calculated with different γSF models. The red band represents the uncertainty arising from different NLD models. Evaluated data from EAF-2010, ENDF/B-VIII.0, JEFF-3.3, and TENDL-2023 libraries are also shown for comparison.

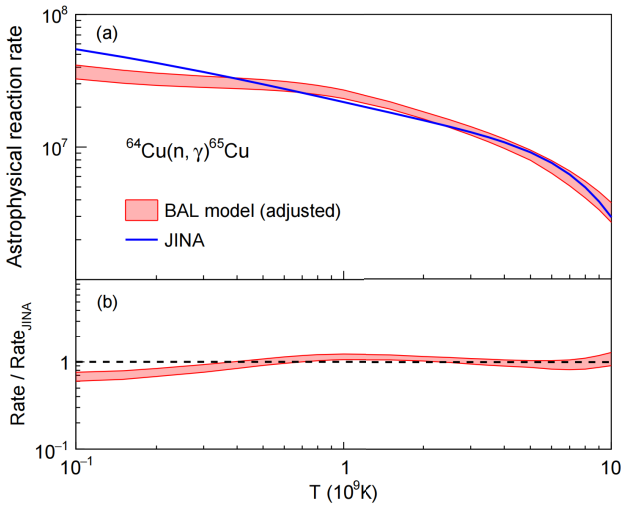

Fig. 9. (color online) Calculated and evaluated astrophysical reaction rates for the ^{64}Cu(n, γ)^{65}Cu reaction (a) and corresponding reaction rate ratio as a function of astrophysical temperature (b).

data from the JINA REACLIB database (using the recommended label *ths8*) [58]. To facilitate comparison, the ratios between the calculated reaction rates and those from from the JINA REACLIB database [58] are shown in Fig. 9(b). In our case, the data uncertainty is also induced by the NLD models, which is not constrained in a proper way due to the lack of experimental ^{64}Cu(n, γ)^{65}Cu data. The comparison shows that our results agree very well with the JINA REACLIB database at astrophysical temperatures over 0.4×10^9, while they are slightly lower at lower temperatures.

V. CONCLUSION

In summary, we have demonstrated a precise measurement of ^{65}Cu(γ, n)^{64}Cu reaction cross sections by using a quasi-monoenergetic, energy-tunable γ-ray beam and high-purity ^{65}Cu target. The ^{65}Cu(γ, n)^{64}Cu data within the energy range of $10.1 \le E_\gamma \le 17.6$ MeV were obtained with a total uncertainty of less than 4%, which is beneficial for resolving the long-standing discrepancy among the existing measurements of this cross section. Furthermore, the ^{65}Cu γSF above S_n was extracted in a reasonable way, and the radiative neutron capture cross sections and astrophysical reaction rates for short-lived ^{64}Cu were calculated and compared with data from several major evaluated nuclear data libraries. It was found that these calculated ^{64}Cu(n, γ)^{65}Cu data exhibit a good agreement with the evaluations.

When employing the adjusted BAL model, the calculated ^{64}Cu γSF shows an overall consistency with the experimental measurement. However, a significant difference still exists between the default calculations and experimental ones, particularly around S_n. This highlights the need for additional experimental constraints on both the γSF and NLD models to reasonably predict (n, γ) cross sections for short-lived isotopes of interest, especially for those nuclei far from stability.

ACKNOWLEDGMENT

We would like to thank the SLEGS and SSRF staffs for their kind support on SLEGS γ-ray beamline operation and ^{65}Cu(γ, n)^{64}Cu *reaction cross section measurement.*

References

[1] T. Kawano, Y. S. Cho, P. Dimitriou *et al.*, Nucl. Data Sheets **163**, 109 (2020)
[2] S. Goriely, P. Dimitriou, M. Wiedeking *et al.*, Eur. Phys. J. A **55**, 172 (2019)
[3] S. Goriely, V. Plujko, Phys. Rev. C **99**, 014303 (2019)
[4] A. J. Koning, D. Rochman, Nucl. Data Sheets **113**(12), 2841 (2012)
[5] M. Herman, R. Capote, B. V. Carlson *et al.*, Nucl. Data Sheets **108**(12), 2655 (2007)
[6] A. Bracco, E. G. Lanza, A. Tamii, Prog. Part. Nucl. Phys. **106**, 360 (2019)
[7] S. Goriely, S. Péru, G. Colò *et al.*, Phys. Rev. C **102**, 064309 (2020)
[8] C. Chen, Y. F. Niu, R. Xu *et al.*, At. Data Nucl. Data Tables **168**, 101770 (2026)
[9] W. Hauser, H. Feshbach, Phys. Rev. **87**, 366 (1952)
[10] E. A. Eliot, D. Hicks, L. E. Beghian *et al.*, Phys. Rev. **94**, 144 (1954)
[11] H. Utsunomiya, T. Renstrøm, G. M. Tveten *et al.*, Phys. Rev. C **98**, 054619 (2018)
[12] L. Katz, A. G. W. Cameron, Can. J. Phys. **29**(6), 518 (1951)
[13] A. D. Antonov, N. P. Balabanov, Y. P. Gangrskii *et al.*, Sov. J. Nucl. Phys. **51**(2), 193 (1990)
[14] S. C. Fultz, R. L. Bramblett, J. T. Caldwell *et al.*, Phys. Rev. B **133**, 1149 (1964)
[15] P. Jiao, Z. R. Hao, Z. C. Li *et al.*, Nucl. Sci. Tech. **36**, 240 (2025)
[16] W. Luo, Nucl. Sci. Tech. **27**, 96 (2016)
[17] S. C. Fultz, B. L. Berman, J. T. Caldwell *et al.*, Phys. Rev. **186**, 1255 (1969)
[18] J. H. He, Z. T. Zhao, Natl. Sci. Rev. **1**, 171 (2014)
[19] R. Z. Tai, Z. T. Zhao, Nucl. Sci. Tech. **35**, 137 (2024)
[20] H. W. Wang, G. T. Fan, L. X. Liu *et al.*, Nucl. Sci. Tech. **33**(7), 87 (2022)
[21] L. X. Liu, H. W. Wang, G. T. Fan *et al.*, Nucl. Sci. Tech. **35**, 111 (2024)
[22] H. H. Xu, H. Utsunomiya, G. T. Fan *et al.*, Nucl. Instrum. Methods Phys. Res. A **1073**, 170249 (2025)
[23] W. Luo, W. Xu, Q. Y. Pan *et al.*, Nucl. Instrum. Methods Phys. Res. A **660**, 108 (2011)
[24] Z. R. Hao, G. T. Fan, H. W. Wang *et al.*, Nucl. Instrum. Methods Phys. Res. A **1013**, 165638 (2021)
[25] Z. R. Hao, H. H. Xu, G. T. Fan *et al.*, Nucl. Instrum. Methods Phys. Res. A **1068**, 169748 (2024)

[26] H. H. Xu, G. T. Fan, H. W. Wang *et al.*, Nucl. Instrum. Methods Phys. Res. A **1033**, 166742 (2022)
[27] H. W. Wang, G. T. Fan, L. X. Liu *et al.*, Nucl. Phys. Rev. **37**(1), 53 (2020)
[28] Z. C. Li, Y. X. Yang, W. Luo *et al.*, Nucl. Instrum. Methods Phys. Res. B **559**, 165595 (2025)
[29] Z. R. Hao, G. T. Fan, H. W. Wang *et al.*, Nucl. Instrum. Methods Phys. Res. B **519**, 9 (2022)
[30] Mesytec GmbH & Co. KG, MDPP-16: Fast high-resolution time and amplitude digitizer, https://www.mesytec.com/products/nuclear-physics/MDPP-16.html (n.d.).
[31] Mesytec GmbH & Co. KG, MVME: VME Data Acquisition Module, https://www.mesytec.com/downloads/mvme.html (n.d.).
[32] L. X. Liu, H. Utsunomiya, G. T. Fan *et al.*, Nucl. Instrum. Methods Phys. Res. A **1063**, 169314 (2024)
[33] B. L. Berman, S. C. Fultz, Rev. Mod. Phys. **47**, 713 (1975)
[34] Z. R. Hao, H. W. Wang, G. T. Fan *et al.*, Sci. Bull. **70**, 2591 (2025)
[35] M. D. Zhou, Z. R. Hao, Q. K. Sun *et al.*, Phys. Rev. C **111**, 054612 (2025)
[36] O. Itoh, H. Utsunomiya, H. Akimune *et al.*, J. Nucl. Sci. Technol. **48**, 834 (2011)
[37] D. M. Filipescu, I. Gheorghe, H. Utsunomiya *et al.*, Phys. Rev. C **90**, 064616 (2014)
[38] T. Renstrøm, H. Utsunomiya, H. T. Nyhus *et al.*, Phys. Rev. C **98**, 054310 (2018)
[39] Z. C. Li, Z. R. Hao, Q. K. Sun *et al.*, Nucl. Sci. Tech. **36**, 34(2025)
[40] G. A. Bartholomew, E. D. Earle, A. J. Ferguson *et al.*, Gamma-Ray Strength Functions, in *Advances in Nuclear Physics, Vol. 7*, edited by M. Baranger and E. Vogt (Boston: Springer US, 1973), p. 229
[41] R. Capote, M. Herman, P. Obložinský *et al.*, Nucl. Data Sheets **110**(12), 3107 (2009)
[42] J. Kristiak, E. Beták, eds., *Neutron Induced Reactions: Proceedings of the 4th International Symposium, Smolenice, Czechoslovakia, June 17–21, 1985* (Dordrecht: Springer Netherlands, 2012)
[43] J. M. Blatt and V. F. Weisskopf, *Theoretical Nuclear Physics* (New York: John Wiley & Sons, 1952)
[44] A. Koning, S. Hilaire, S. Goriely, Eur. Phys. J. A **59**, 131 (2023)
[45] D. M. Brink, Nucl. Phys. **4**, 215 (1957)
[46] P. Axel, Phys. Rev. **126**, 671 (1962)
[47] E. B. Balbutsev, I. V. Molodtsova, P. Schuck, Nucl. Phys. A **872**, 42 (2011)
[48] R. Roussel, A. L. Edelen, T. Boltz *et al.*, Phys. Rev. Accel. Beams **27**, 084801 (2024)
[49] S. Jalas, M. Kirchen, P. Messner *et al.*, Phys. Rev. Lett. **126**, 104801 (2021)
[50] A. Gilbert, A. G. W. Cameron, Can. J. Phys. **43**, 1446 (1965)
[51] W. Dilg, W. Schantl, H. Vonach *et al.*, Nucl. Phys. A **217**, 269 (1973)
[52] A. V. Ignatyuk, K. K. Istekov, G. N. Smirenkin, Yadernaya Fizika **29**(4), 875 (1979)
[53] A. V. Ignatyuk, J. L. Weil, S. Raman *et al.*, Phys. Rev. C **47**, 1504 (1993)
[54] M. Samyn, S. Goriely, M. Bender *et al.*, Phys. Rev. C **70**, 044309 (2004)
[55] S. Hilaire, S. Goriely, Nucl. Phys. A **779**, 63 (2006)
[56] S. Hilaire, M. Girod, S. Goriely *et al.*, Phys. Rev. C **86**, 064317 (2012)
[57] H. Utsunomiya, T. Renstrøm, G. M. Tveten *et al.*, Phys. Rev. C **100**, 034605 (2019)
[58] R. H. Cyburt, A. M. Amthor, R. Ferguson *et al.*, ApJS **189**(1), 240 (2010)